Hydrogel Microcapsules with a Thin Oil Layer: Smart Triggered Release via Diverse Stimuli

Hye-Seon Jeong, Eunseo Kim, Changwoo Nam, Yoon Choi, You-Jeong Lee, David A. Weitz, Hyomin Lee,* and Chang-Hyung Choi*

A hydrogel microcapsule with an intermediate thin oil layer is presented to achieve smart release of a broad range of cargoes triggered via diverse stimuli. A microfluidic technique is used to produce triple emulsion droplets with a thin oil layer that separates the innermost aqueous phase from the hydrogel prepolymer phase, which transforms into a hydrogel shell via photopolymerization. The intermediate oil layer within the hydrogel microcapsule acts as an effective diffusion barrier, allowing encapsulation of various small cargoes within a porous hydrogel shell until a stimulus is applied to destabilize the oil layer. It is demonstrated that diverse stimuli including chemical dissolution, mechanical stress, and osmotic pressure can be utilized to release the encapsulated cargo on-demand. In addition, osmotic pressure and the hydrogel shell thickness can be independently tuned to control the onset time of release as well as the release behavior of multi-cargo encapsulated hydrogel microcapsule. The release can be either simultaneous or selective.

1. Introduction

Smart microcapsules have important applications in various fields including food,[1] cosmetics,[2] home-care,[3] personal-care,[4] and biomedicine,[5] due to their ability to effectively store and release the encapsulated materials upon exposure to various stimuli such as pH,[6] temperature,[7] mechanical

H.-S. Jeong, Y. Choi, Y.-J. Lee, Prof. C.-H. Choi
Division of Cosmetic Science and Technology
Daegu Haany University
1 Haanydaero, Gyeongsan, Gyeongbuk 38610, Korea
E-mail: cchoi@dhu.ac.kr
E. Kim, Prof. C. Nam, Prof. H. Lee
Department of Chemical Engineering
Pohang University of Science and Technology (POSTECH)
77 Cheongam-Ro, Nam-Gu, Pohang, Gyeongbuk 37673, Korea
E-mail: hyomin@postech.ac.kr
Prof. C. Nam
Organic Materials and Fiber Engineering
Jeonbuk National University
567 Baekje-daero, Deokjin-gu, Jeonju, Jeollabuk-do 54896, Korea
Prof. D. A. Weitz
John A. Paulson School of Engineering and Applied Sciences
and Department of Physics
Harvard University
9 Oxford St, Cambridge, MA 02138, USA

pressure,[8] and chemical agents.[9] These stimuli-responsive microcapsules are typically produced from emulsion droplets, in which the dispersed phase serves as a template in preparing either solid polymeric microspheres or a rigidified membrane of a core-shell structured microcapsule by various chemical or physical approaches such as polymerization,[10] interfacial complexation,[11] host–guest interaction,[12] phase change,[13] and solvent evaporation.[14]

Recent advances in droplet microfluidics enable precise control of multiphase flows, leading to high throughput production of monodisperse multi-phase emulsion droplets with fine-tunable sizes, morphologies, and compositions.[15] These multiple emulsions can be readily converted to microcapsules with tailored physical and chemical properties for controlled release of encapsulated materials. For instance, double emulsions with a middle phase that separates the inner droplet from the outer continuous phase have been used to encapsulate hydrophilic or hydrophobic actives by utilizing either water-in-oil-in-water (W/O/W) or O/W/O emulsion droplets, respectively. While consolidation of the intermediate phase in each system allows generation of a solidified shell membrane that can be fine-tuned to achieve triggered release of encapsulated materials through various external stimuli,[16] these systems each have several drawbacks; for example, the hydrophobic nature of the shell membrane is often incompatible with biomolecules such as proteins in W/O/W templated microcapsules, while O/W/O templated microcapsules are only applicable to encapsulation of hydrophobic actives.[17] Alternatively, even higher-order multiple emulsions, such as triple emulsion droplets have been proposed recently as a promising capsule template to overcome these issues.[18] The distinctive feature of the resulting capsules formed from triple emulsion droplets is an additional intermediate layer that separates the outer capsule shell from the innermost droplet. For instance, by using either an ultra-thin water layer or a cross-linked hydrogel layer in an O/W/O/W triple emulsion droplet, high encapsulation efficiency and long-term storage of volatile hydrophobic cargo within a hydrophobic polymeric shell was achieved.[19] A broad range of polar and non-polar cargoes have also been encapsulated in a single platform by utilizing omniphobic fluorocarbon oil as the intermediate layer.[20] Both of these studies primarily focused on the encapsulation and retention of various

cargo materials. Interestingly, the presence of two intermediate layers offers a new opportunity to independently tune each layer to achieve multicomponent encapsulation and stimuli-responsiveness in a single platform. However, this potential has never been explored.

In this work, we report a versatile hydrogel microcapsule with a thin oil layer to achieve smart release of a broad range of cargoes triggered via diverse stimuli. Using a capillary microfluidic device, we produce monodisperse triple emulsion droplets, enveloping an ultra-thin oil layer in between the innermost aqueous phase and the aqueous hydrogel pre-polymer phase, which transforms into a hydrogel shell upon UV illumination. In addition, we demonstrate the on-demand release of the encapsulated cargo within the microcapsule by destabilizing the interstitial oil layer via diverse stimuli such as chemical dissolution, mechanical stress, and osmotic pressure while the hydrogel shell remains intact. Furthermore, we achieve either simultaneous or selective release of cargoes in a dual component encapsulated hydrogel microcapsule by tuning the hydrogel shell thickness and thus the mechanical properties of the hydrogel shell.

2. Results and Discussions

2.1. Microfluidic Production of Hydrogel Microcapsules with a Thin Oil Layer for Encapsulation of Various Hydrophilic Cargoes

To make these hydrogel microcapsules with a thin oil layer, we utilize triple emulsion droplets as templates, as shown in **Figure 1**A,B. The triple emulsion droplets are prepared using a glass capillary microfluidic device. To produce triple emulsion droplets, an aqueous solution containing hydrophilic actives is supplied through the small tapered capillary. An oil phase containing surfactant is supplied through the injection capillary to form a periodic stream of large aqueous droplets in the oil phase due to the preferential wetting of the oil phase onto the wall of the hydrophobically treated injection capillary. This allows formation of a lubrication layer between the innermost aqueous droplet and the wall of the injection capillary, resulting in formation of a thin oil layer within each triple emulsion droplet upon emulsification process. Next, additional aqueous hydrogel prepolymer solution, comprising of 10% poly(ethylene glycol) diacrylate (PEGDA), surfactant (2% poly(vinyl alcohol) (PVA)), and photoinitiator, is supplied through the interstices between the injection capillary and the square capillary in a co-flow manner. The tri-phasic coaxial flow is emulsified at the entrance of the collection capillary by the shearing of the outer oil phase (2% Span80 in mineral oil), forming highly uniform triple emulsion droplets with a thin oil layer. These triple emulsion droplets are converted into hydrogel microcapsules via UV-induced polymerization at the end of the tubing, as evidenced by the optical and fluorescence micrographs of Figure S1, Supporting Information. Then, the hydrogel microcapsules dispersed in the oil phase are transferred into water phase without any extra washing steps by direct collection in water. This is due to large density difference between the hydrogel microcapsule and the oil phase as well as strong affinity of the hydrogel to water, as shown in Figure 1C,D. We also note that the

discontinuous nature of the innermost aqueous droplet in the inner oil phase during droplet formation results in production of both W/O/W/O triple emulsion droplets as well as O/W/O double emulsion droplets; the estimated production yield for the triple emulsion droplets is approximately 85%. However, hydrogel capsules templated from O/W/O double emulsion droplets exhibit an average density lower than that of water and thus it is very easy to separate and remove them when they are transferred to water. Moreover, the overall size as well as the shell thickness of the microcapsules can be readily tuned by varying the flow rates of the inner and the continuous phase that are supplied through the injection capillary as shown in Figure S2, Supporting Information.

The presence of an intermediate oil layer within the hydrogel microcapsule allows encapsulation of a broad range of hydrophilic cargoes within the aqueous core of the hydrogel microcapsules. To validate this, we first demonstrate that small actives such as erioglaucine (blue dye, 793 Da) and fluorescein sodium salt (green dye, 376 Da) can be encapsulated within an oil layer in the hydrogel microcapsule. Moreover, by choosing an oil layer comprising of hexadecane and surfactant, both hydrophilic cargoes exhibited long term retention up to 3 months revealing that the oil layer serves as an excellent barrier layer as shown in the optical and fluorescence micrographs of Figure 1E,F. To further extend the applicability of these hydrogel microcapsules, we encapsulate proteins with hydrophobic moieties that are known to readily adsorb at an oil/water interface and easily denature over time.[21] By utilizing a fluorocarbon oil with suitable surfactant (2% Krytox-PEG-Krytox in FC-70) as the thin oil layer, we successfully encapsulate fibrinogen in an efficient and biocompatible manner,[20] as shown in Figure 1G. We also encapsulate colloids (2 μm diameter) in the hydrogel microcapsule with one order less in the amount of surfactant in the fluorocarbon oil layer. The reduction in the amount of surfactant in the fluorocarbon oil phase results in an increase in the value of the interfacial tension with the adjacent phases and thus significant reduction in the stability of the intermediate oil layer.[22] This leads to dewetting of the fluorocarbon oil layer over time and formation of destabilized droplet within the hydrogel microcapsules as shown in Figure 1H. While tuning the surfactant concentration in the oil layer allows modulation of the intermediate layer stability, the onset point at which the destabilization occurs is difficult to control precisely.

2.2. On-Demand Release of Encapsulated Cargo in Hydrogel Microcapsules via Diverse Stimuli

The ability to selectively and controllably induce destabilization of the intermediate oil layer, without altering the hydrogel shell, has great potential for on-demand release of hydrophilic cargoes encapsulated in microcapsules. To demonstrate this, we prepare sets of microcapsules with a thin oil layer encapsulating a model cargo (Alexa Fluor 594). We note that for all the microcapsules prepared, 10% PEGDA, 2% PVA, and photoinitiator was used for the aqueous hydrogel precursor phase to produce a hydrogel shell with an estimated mesh size of 2 nm.[23] This is larger than the hydrodynamic diameter of Alexa Fluor 594,
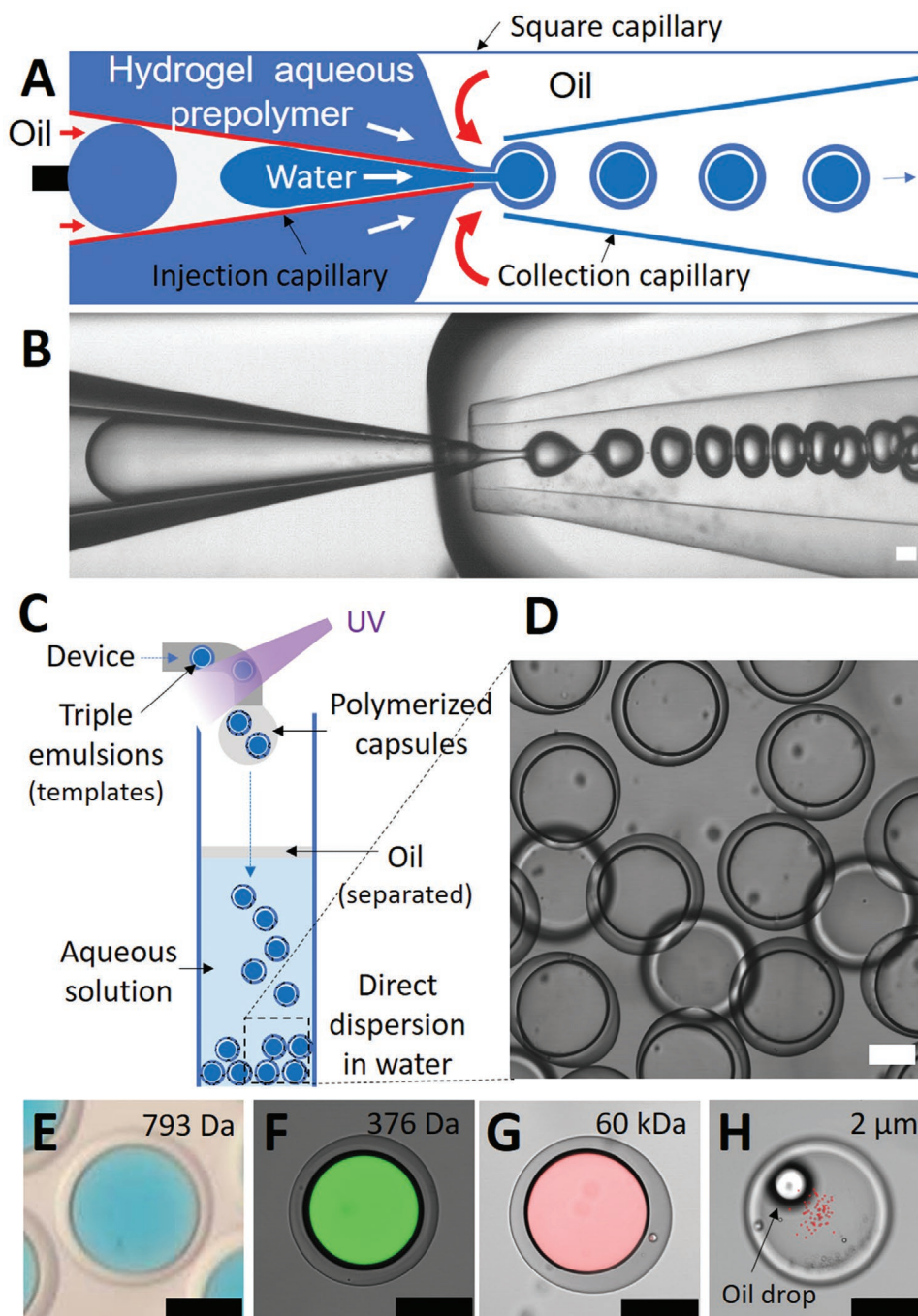
Figure 1. Microfluidic production of hydrogel microcapsules with a thin oil layer to encapsulate various hydrophilic cargoes. A) A schematic showing a glass capillary microfluidic device for generation of water-in-oil-in-water-in-oil (W/O/W/O) triple emulsion droplets. B) Bright-field micrograph showing continuous production of emulsion droplets. C) A schematic showing collection of hydrogel microcapsules directly in water without extra washing step. D) Bright-field micrograph showing the collected monodisperse hydrogel microcapsules in water. E–H) Bright-field and confocal micrographs of hydrogel microcapsules encapsulating various hydrophilic cargoes. E) Erioglaucine (blue), F) Fluorescein sodium salt (green), G) Rhodamine isothiocyanate (RITC)-fibrinogen (Alexa Fluor 647 fibrinogen, red), and H) Colloids (FluoSphere, red). All scale bars represent 100 μm.

which is 1.48 nm.[24] This allows direction visualization of the cargo release through the hydrogel shell upon destabilization of the thin oil layer comprising of hexane.

To first demonstrate the cargo release upon dissolution of the oil layer, we suspend the hydrogel microcapsules with a hexane oil layer in an aqueous solution containing 20% ethanol; this initiates the dissolution of the oil layer since hexane is miscible with ethanol. During this process, we observe that the microcapsules temporarily become larger in size for a short period (within 2 min) possibly due to influx of water and
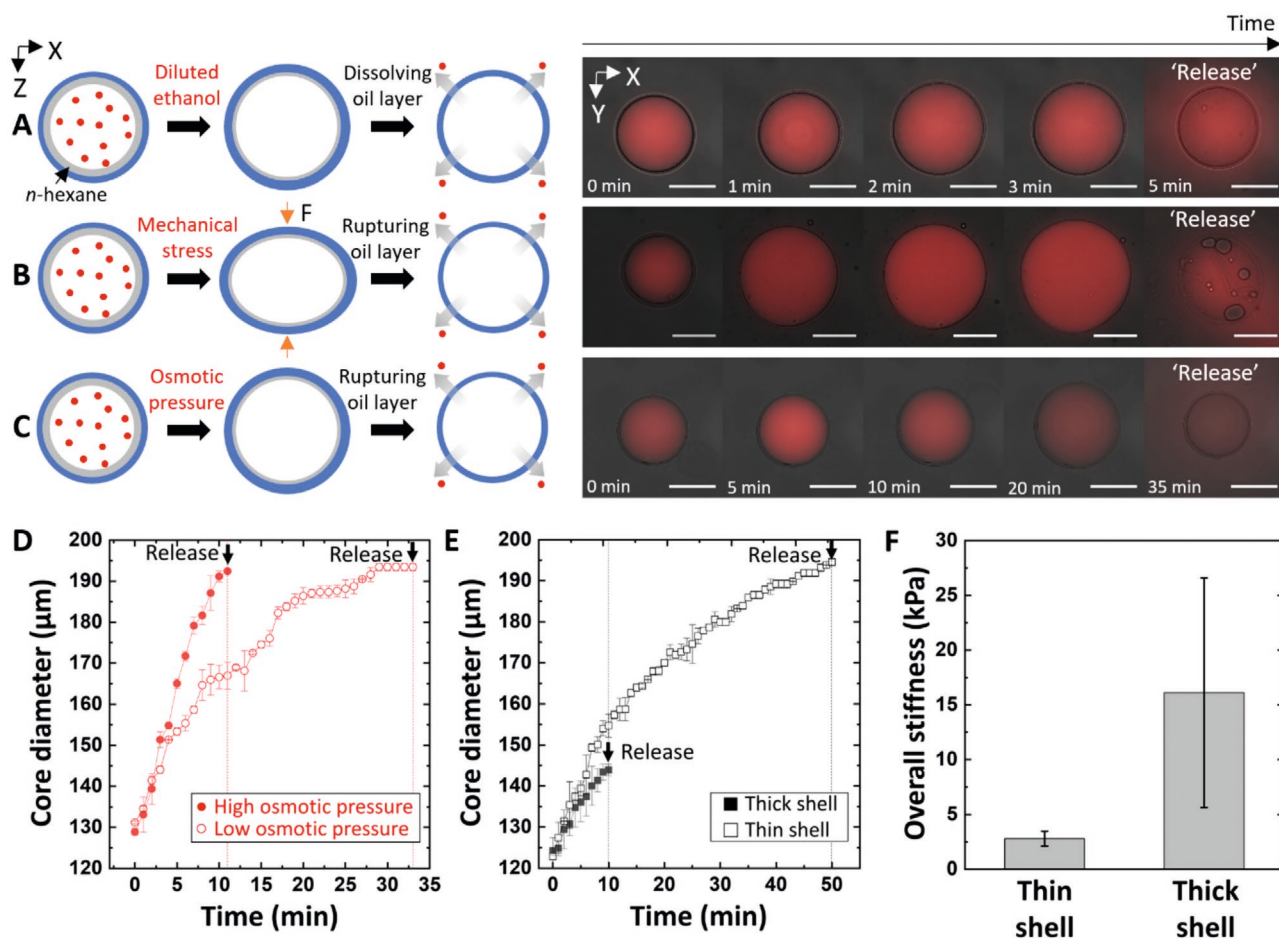
**ADVANCED
SCIENCE NEWS**
www.advancedsciencenews.com

**ADVANCED
FUNCTIONAL
MATERIALS**
www.afm-journal.de

Figure 2. On-demand release of encapsulated cargo within the hydrogel microcapsules by selectively destabilizing the interstitial oil layer via diverse external stimuli such as, A) dissolution, B) mechanical pressure, and C) osmotic pressure while the hydrogel shell remains intact. The oil layer within the microcapsule comprises of n-hexane. D) The effect of osmotic pressure on the core size of a thin shell hydrogel microcapsule versus time. E) The effect of shell thickness on the core size of a hydrogel microcapsule versus time. F) The effect of shell thickness on the overall stiffness of the hydrogel microcapsules. All scale bars represent 100 μm.

ethanol through the hydrogel shell and the intermediate oil layer (hexane). However, upon rapid dissolution of the intermediate oil layer, the microcapsule releases the encapsulated cargo through the hydrogel shell (within 30 min) and contracts as shown in **Figure 2**A. We also note that similar release behavior due to dissolution of the oil layer is observed for hydrogel microcapsules with a hexadecane oil layer as shown in Figure S3A, Supporting Information (see also Movie S1, Supporting Information).

To investigate the effect of mechanical pressure imposed on the microcapsule, we place the hydrogel microcapsules with a hexane oil layer between two glass slides with an excess amount of water. Upon evaporation of the excess water between the two glass slides, the compressive pressure exerted by the top glass on the microcapsule increases, leading to lateral expansion of the microcapsule. Further increase in pressure yields rupture of the oil layer and subsequent release of the cargo due to compressive pressure as shown in Figure 2B. This is also applicable to hydrogel microcapsules with FC-70 as the thin oil layer, demonstrating the high flexibility and robustness of our proposed microcapsules to accomplish smart release system

via diverse stimuli as shown in Figure S3B (see also Movie S2, Supporting Information).

Then, to determine the effect of osmotic pressure on the microcapsule, we prepare hydrogel microcapsules with a hexane oil layer containing the model cargo and 10% sucrose in the aqueous core and monitor the release behavior upon exposure to DI water as shown in the sequential fluorescence micrographs of Figure 2C. When the microcapsules are dispersed in DI water, the hypotonic condition of the continuous phase drives water to diffuse through the oil layer, which serves as a semi-permeable membrane, and into the aqueous core. We note that while oil is immiscible with water, water can be still transported through the oil layer in reverse micelle form or via hydrated surfactants under osmotic pressure gradient depending on the composition and the thickness of the oil layer.[25] Moreover, hydrogel shell is permeable to sucrose as the hydrodynamic diameter of sucrose is 0.9 nm and thus smaller than the mesh size of the hydrogel shell.[26] The influx of water causes the aqueous core to expand in volume and the oil layer destabilizes over time resulting in the cargo release through the hydrogel shell as shown in schematics of Figure 2C. One

ADVANCED
SCIENCE NEWS
www.advancedsciencenews.com

ADVANCED
FUNCTIONAL
MATERIALS
www.afm-journal.de

of the major advantages of utilizing osmotic pressure as a cue for cargo release lies in the fact that the osmotic pressure can be tuned precisely by either altering the osmolyte concentration in the aqueous core or the continuous phase to which the microcapsules are exposed. More importantly, the osmotic pressure imposed on the microcapsule allows manipulation of the time at which the oil layer starts to destabilize and initiate the release of cargo. To validate this hypothesis, we prepare two sets of identical microcapsules containing 20% sucrose in the aqueous core and disperse one set in DI water and the other in an aqueous solution containing 5% sucrose. The osmolarity of each continuous phase is 0 and 160 mOsmol kg^{-1}, respectively, while the aqueous core containing 20% sucrose, surfactant, and the cargo yields 871 mOsmol kg^{-1}. Then, we monitor the change in the innermost core diameter as a function of time and determine the point at which the cargo is released from the microcapsule as shown in the plot of Figure 2D. We observe that the microcapsules dispersed in DI water start to release the cargo within 10 min while the capsules dispersed in 5% sucrose solution exhibit more than a threefold increase in the onset time of release, as evidenced by the plot of Figure 2D. This result confirms that the extent of osmotic pressure imposed on the hydrogel microcapsule can be varied to tune the onset time of cargo release.

To clearly verify the origin of this osmotic pressure-triggered release of cargo in hydrogel microcapsules, we prepare another two sets of microcapsules both containing 10% sucrose in the aqueous core but with varying shell thickness; one has the same shell thickness as the microcapsules described previously with a thickness of approximately 6 μm (denoted as thin shell) while the other has approximately 17 μm (denoted as thick shell). Under the same hypotonic condition and thus the same extent of osmotic pressure imposed on the oil layer, the thin shell microcapsule expands much faster in the core diameter compared to the analogous microcapsules with a thicker shell as shown in the plot of Figure 2E. This distinct core expansion behavior in these microcapsules arises from the different mechanical response of the hydrogel microcapsules.

To determine the mechanical property of the hydrogel microcapsule with varying shell thicknesses, we employ the micropipette-aspiration method (Figures S4 and S5, Supporting Information). While there are several models reported previously that enable estimation of the modulus of a hydrogel shell with a layered structure,[27] we determine the overall stiffness of the microcapsule from the slope of the deformation curve. Since we are interested in the deformation of microcapsule under pressure differential,[28] the curve denotes to the extent of capsule deformation divided by the inner pipette radius with respect to the applied pressure differential as shown in the plot of Figure S6, Supporting Information. As the aqueous core of the microcapsule has a negligibly low modulus compared to the hydrogel shell, the overall stiffness of the microcapsule is directly related to the hydrogel shell thickness. The overall stiffnesses of the thin shell and thick shell microcapsule are 2.78 ± 0.69 kPa and 16.12 ± 10.48 kPa, respectively, as shown in the plot in Figure 2F. This result confirms that the water influx rate and thus the rate of core expansion is inversely proportional to hydrogel shell thickness at a given osmotic pressure and thus the thin shell microcapsule exhibits faster rate of expansion

than the thick shell-microcapsule. However, in-depth examination of the data in Figure 2E reveals that the encapsulated cargo in the thick shell microcapsule is released within 10 min with small variance in the aqueous core size while the cargo is released after 50 min for the thin shell microcapsule with relatively larger extent of core expansion. This rather counterintuitive behavior is due to the effective stress imposed on the oil layer. While same extent of osmotic pressure is imposed on the semi-permeable oil layer, the water influx rate depends on both the osmotic pressure as well as the stiffness of the hydrogel shell. As the shell stiffness increases, it requires more energy to deform and thus the water influx rate as well as the rate of core expansion at a given osmotic pressure is slower for thick shell-microcapsules with higher stiffness compared to thin shell microcapsule.[29] As a result, the thick shell microcapsule with slower water influx rate is less effective in relieving the osmotic pressure imposed on the oil layer. Therefore, the effective stress imposed on the oil layer within the thick shell microcapsule is much higher than the thin shell-microcapsule causing the oil layer in the thick shell microcapsule to destabilize earlier and at a smaller core diameter. These results reveal the unique characteristics of the hydrogel microcapsule with an oil layer in which the oil layer serve as a semi-permeable membrane while the hydrogel shell acts as the rate modulator for water influx via its tunable overall stiffness. However, at the same time, we note that the intermediate oil layer within these microcapsules should also exhibit sufficient robustness, avoiding any unintended release of encapsulated cargo under moderate mechanical perturbation. To confirm where these microcapsules with a thin oil layer are stable to external stress, we first prepared a set of microcapsules under isotonic condition; these microcapsules were stable over a week without any leakage as shown in the series of fluorescence micrographs of Figure S7, Supporting Information. Then, we monitored these capsules under high external shear conditions such as vortexing to find that all the microcapsules were intact with near 100% fidelity (Figure S8, Supporting Information). Furthermore, we conducted additional experimentations to verify the effect of mild osmotic pressure on the thin oil layer stability within the microcapsule. For this experiment, we prepared microcapsules containing 0.20% aqueous solution of sucrose in the innermost aqueous core (6 mOsmol kg^{-1}), and these capsules were dispersed in an 0.15% aqueous solution of sucrose (4 mOsmol kg^{-1}). We observe that in such mild osmotic pressure condition, the microcapsule becomes a bit larger in size but eventually plateaus and remains stable after reaching osmotic equilibrium as shown in Figure S9, Supporting Information. Combined, these results indicate that the thin oil layer within our hydrogel microcapsules has sufficient robustness to fully benefit the advantage to release the encapsulated cargo on-demand.

2.3. Smart Controlled Release of Multiple Cargoes in Hydrogel Microcapsules with a Thin Oil Layer

The presence of two intermediate layers, the inner oil layer and the outer hydrogel shell layer, in the hydrogel microcapsule offers new opportunities to achieve either selective or simultaneous release of encapsulated multiple cargoes. To

**ADVANCED
SCIENCE NEWS**
www.advancedsciencenews.com

**ADVANCED
FUNCTIONAL
MATERIALS**
www.afm-journal.de

first validate the capability of multicomponent encapsulation in a single hydrogel microcapsule, we incorporate two types of model hydrophilic cargoes, Fluorescein isothiocyanate–dextran (FITC-dextran, green) and Alexa Fluor 594 (red), respectively, with drastically different hydrodynamic radius in the hydrogel

microcapsule. We observe that both cargoes are successfully encapsulated within the hydrogel microcapsules, as shown in brightfield as well as the fluorescence composite micrographs of **Figure 3**A. In a separate experiment, we prepare two sets of microcapsules both containing the two cargoes and 10%
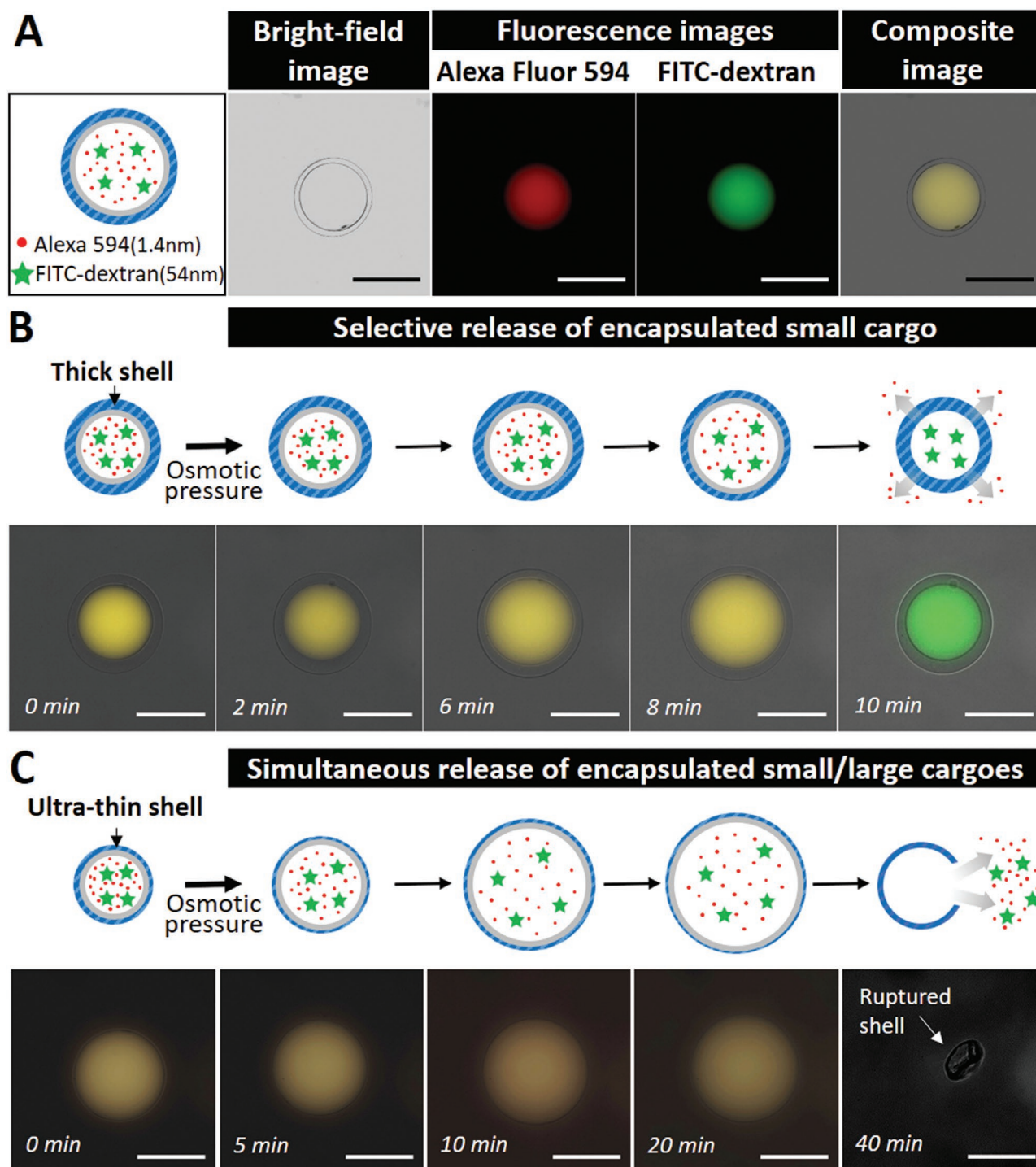

Figure 3. Smart controlled release of multiple cargoes encapsulated within the hydrogel microcapsules either in a selective or a simultaneous manner. A) Brightfield-fluorescence composite micrographs showing co-encapsulation of two hydrophilic cargoes (Alexa Fluor 594 and FITC-dextran) in the microcapsule. Sequential composite micrographs showing B) selective release of the smaller cargo (Alexa Fluor 594) and C) simultaneous release of both cargoes by rupturing of the hydrogel shell via osmotic pressure-induced water influx (under hypotonic condition). All scale bars represent 100 µm.

**ADVANCED
SCIENCE NEWS**
www.advancedsciencenews.com

**ADVANCED
FUNCTIONAL
MATERIALS**
www.afm-journal.de

sucrose in the aqueous core but with varying hydrogel shell thicknesses; one has shell thickness of approximately 15 μm (thick) whereas the other has a shell thickness of approximately 1 μm (ultra-thin). Then, we monitor the behavior of each set of microcapsules with different shell thicknesses upon transfer to a hypotonic condition (DI water), as shown in the schematic illustration and the corresponding series of fluorescence micrographs in Figure 3B,C.

For the thick shell microcapsule, the aqueous core expands and the thin oil layer ruptures within 10 min, as evidenced by the change of florescence signal in the core from yellowish green to green color due to selective release of Alexa Fluor 594 (red) as shown in the sequential composite fluorescence micrographs of Figure 3B. Due to the stiff nature of the thick shell microcapsule, the hydrogel shell remains intact under the osmotic pressure imposed and only the Alexa Fluor 594 which is smaller than the mesh size of the hydrogel shell, is selectively released while the larger-sized FITC-dextran remains within the microcapsule.

In contrast, when an analogous ultra-thin shell microcapsule is exposed to the same hypotonic condition, the influx of water causes expansion of the aqueous core, leading to concurrent expansion of the ultra-thin hydrogel shell. This is followed by yielding and ultimately rupture of the hydrogel shell within 35 min, as evidenced by the simultaneous release of both model cargoes in the composite micrographs of Figure 3C. We note that while the overall stiffness of this ultra-thin hydrogel microcapsule was not obtainable using the current micropipette aspiration setup due to the rapid and sensitive response of the ultra-thin microcapsules, we observe consistent and reproducible behavior among these two sets of microcapsules with different shell thickness as shown in the plot of Figure S10, Supporting Information. Overall, these results imply that even under the same osmotic pressure and with the same composition of the hydrogel shell, the shell thickness and thus the overall stiffness can be tuned in hydrogel microcapsules containing multiple components to implement the release profile to be in a selective or simultaneous manner.

2.4. Biocompatible Hydrogel Microcapsules for Anti-Cancer Drug Delivery Applications

Recently, mechano-responsive microcapsules are gaining significant attention as they are applicable to diverse fields including encapsulation and controlled release of fragrances,[30] nutrient preservation,[31] self-healing adhesives,[32] and even stem cell therapy.[8a] To extend the applicability of our biocompatible hydrogel microcapsules with controlled release behavior in drug delivery systems, we first incorporate water-soluble anti-cancer drug, doxorubicin hydrochloride (1 mg mL^{-1}) and 10% sucrose in the innermost aqueous phase of a thick shell microcapsule (average shell thickness: 12 μm), as schematically shown in **Figure 4**A. Doxorubicin (543 g mol^{-1}, 1.5 nm)[33] is similar in size to Alexa Fluor 594 (819 g mol^{-1}, 1.5 nm) and is inherently fluorescent, enabling visualization of their release behavior through the hydrogel shell via fluorescence microscopy. We also note that soybean oil is used for the thin oil layer to improve their biocompatibility. We observe that while the

microcapsules remain intact in isotonic condition, exposure to hypotonic condition results in the aqueous core to expand, thereby leading to release of doxorubicin through the hydrogel shell by rupture of the oil layer, as shown in the sequential fluorescence micrographs of Figure 4Ba,b,c,d.

The ability to precisely control the amount of drug released at the target site is one of the major challenges in controlled drug delivery systems.[34] As microfluidics enable consistent production of highly monodisperse microcapsules with pre-defined amount of drug in each microcapsule, the capsule number concentration can be varied to control the concentration of the drug released. To validate this hypothesis, we prepare five sets of microcapsule suspension with varying number concentration; each suspension contains different number of microcapsules dispersed in the same volume of DI water. Similarly, the osmotic pressure imposed causes the thin oil layer in the microcapsules to rupture and the encapsulated doxorubicin to release into the media. We observe a linear correlation between the doxorubicin concentration in the media and the capsule number concentration as shown in the plot of Figure 4C and Figure S11, Supporting Information (standard curve), demonstrating the potential of hydrogel microcapsules in tuning the drug concentration at the target site by simply varying the number of microcapsules applied.

Next, to exploit the release behavior of ultra-thin shell microcapsules in drug delivery systems, we incorporate two anti-cancer drugs with different polarity in a single microcapsule, as schematically shown in Figure 4D. Encapsulation of both hydrophilic and hydrophobic drugs in a single microcarrier has great potential in providing synergistic benefits as two or more actives can be simultaneously released in desired dosages at the target site;[35] this is particularly important for fatal diseases such as cancer or human immunodeficiency virus, where cocktails of drug is required. To demonstrate the simultaneous release of two common anti-cancer drugs by osmotic pressure, we prepare microcapsules with an ultra-thin hydrogel shell (average shell thickness: 2.5 μm) containing doxorubicin (red, 1 mg mL^{-1}) in the aqueous core and Oregon green dye labelled paclitaxel (green, 40 μg mL^{-1}) in the soybean oil layer, as shown in the composite fluorescence micrographs of Figure 4E. Upon applying osmotic pressure, the influx of water causes expansion of the aqueous core, followed by rupture of the hydrogel shell prior to the oil layer. This leads to release of doxorubicin and paclitaxel, as evidenced by the decrease of the red fluorescence signal into the surrounding aqueous solution and formation of green fluorescent oil droplet in the composite fluorescence micrographs of Figure 4E. While doxorubicin is released rapidly into the aqueous media upon rupture of the hydrogel shell (Figure 4E-d), paclitaxel is relatively slowly released from the oil drop (Figure 4E-e) due to low solubility of paclitaxel in water (0.3 μg mL^{-1}).[36] To confirm this, we carried out a separate set of experiments to examine the release behavior of paclitaxel from an oil drop comprising of soybean oil. For these experiments, we prepared four aqueous samples (1 mL) containing an oil drop (3 μL) with varying concentration of paclitaxel and monitored the accumulated amount of paclitaxel released in aqueous media via UV-VIS spectrophotometer (λ_{max} = 227 nm). Within the concentration range tested, we observe that paclitaxel slowly releases into the aqueous media from the oil drop and that the

**ADVANCED
SCIENCE NEWS**
www.advancedsciencenews.com

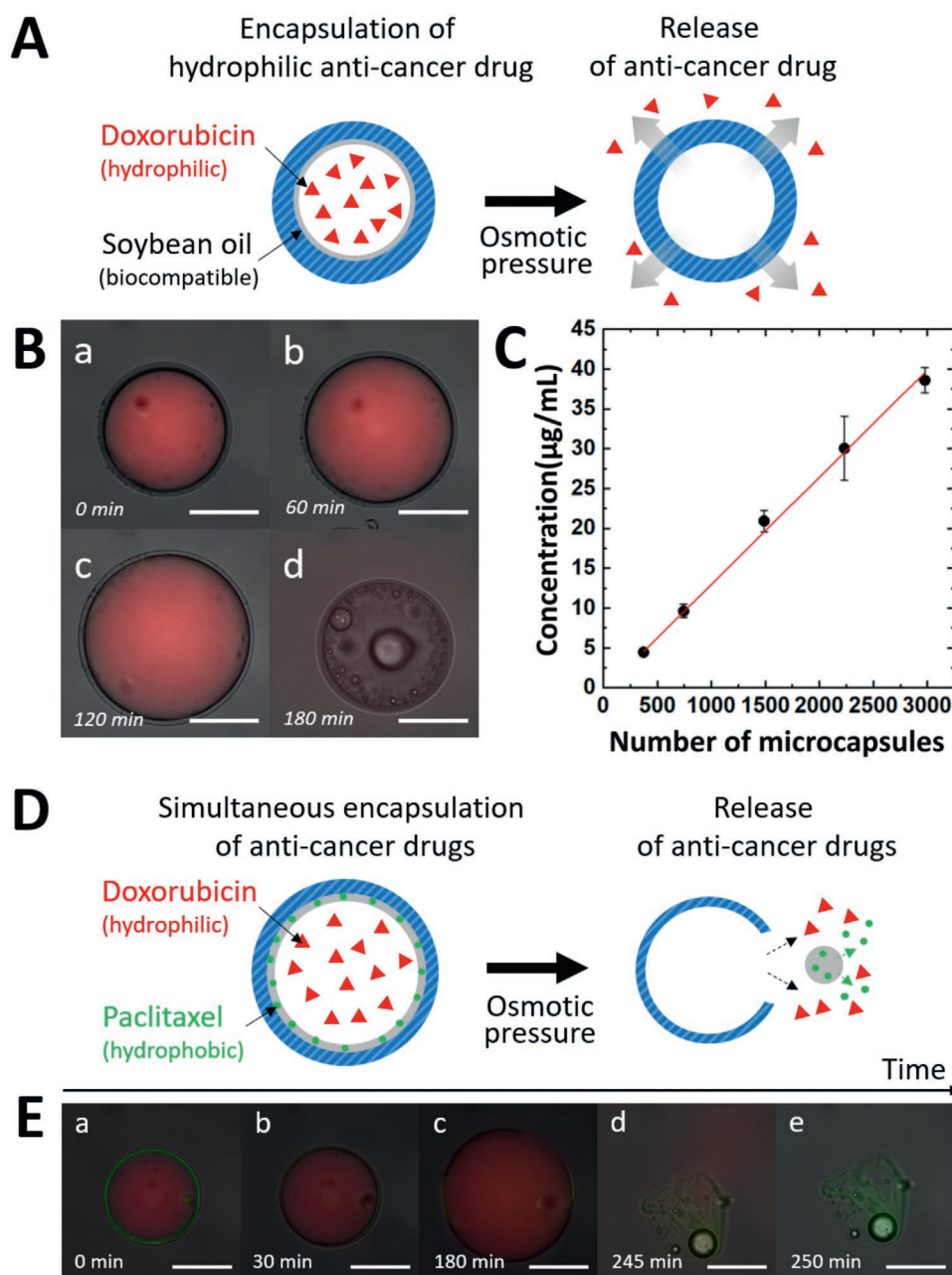**ADVANCED
FUNCTIONAL
MATERIALS**
www.afm-journal.de

Figure 4. Biocompatible hydrogel microcapsules for anti-cancer drug delivery applications. A) Schematics showing the encapsulation and osmotic pressure-induced release of doxorubicin in a thick-shell microcapsule. B) Sequential fluorescence micrographs showing the release of doxorubicin through the hydrogel shell by rupture of the oil layer. C) A plot of the doxorubicin concentration in the media versus the capsule number concentration. D) Schematics showing the simultaneous encapsulation and osmotic pressure-induced release of doxorubicin and paclitaxel in an ultra-thin shell microcapsule. E) Composite fluorescence micrographs showing release of doxorubicin and paclitaxel by rupture of the hydrogel shell. All scale bars represent 100 μm.

amount of paclitaxel released is proportional to the initial concentration of paclitaxel in the oil drop until it reaches close to the reported saturation limit in water (≈0.2 μg mL^{-1}) as shown in the plot of Figure S12, Supporting Information.

We also note that these hydrogel microcapsules with a soybean oil layer rupture within 180 min while analogous microcapsules with a hexane oil layer presented earlier rupture within 35 min when same extent of osmotic pressure is imposed. We

believe that this is due to the higher viscosity of soybean oil (40.5 cP)[37] compared to hexane (0.28 cP).[38] The higher viscosity of the oil phase not only results in thicker oil layer within the hydrogel microcapsule during droplet formation but also slower transport of water through this oil layer.

Osmotically driven water transport through an oil layer occurs in the form of inverse micelles, tiny water droplets, and hydrated surfactants that diffuse through the oil layer.[39]

It has been previously reported that the time required for the structural change of the oil layer before the apparent water transport starts (also known as the lag time) increases as the viscosity of the oil layer in water-in-oil-water (W/O/W) double emulsion increases.[40] Moreover, the increment of viscosity decreases the diffusion rate of inverse micelles, tiny water droplets, and hydrated surfactants. These variations in kinetic transport parameters (thickness, viscosity) may lead to slower water transport in soybean oil layer compared to hexane and thus substantially longer time for the capsule to rupture when same extent of osmotic pressure is imposed.

To verify the oil layer thickness for ultra-thin hydrogel microcapsules comprising of either hexane or soybean oil, we conducted additional experimentations. For this experiment, we measured the oil droplet volume upon rupture for each microcapsule and estimated the oil layer thickness using the model reported previously.[41] Based on this calculation, we find that the ultra-thin hydrogel microcapsules containing hexane with less viscosity exhibit an oil layer thickness of approximately 0.1 µm while analogous microcapsules containing soybean oil have 1.1 µm. This result reveals that the hydrogel microcapsules with a soybean oil layer may rupture slower due to higher viscosity and thicker oil layer which leads to slower water transport.

3. Conclusion

Here, we present a microfluidic approach to prepare hydrogel microcapsules with a thin oil layer, allowing multicomponent encapsulation of broad range of cargoes. In addition, we demonstrate that the intermediate oil layer within the hydrogel microcapsule enables on-demand release of the encapsulated cargo upon destabilization of the oil layer via diverse stimuli such as chemical dissolution, mechanical stress, and osmotic pressure while the hydrogel shell remains intact. Among these various cues, osmotic pressure can be fine-tuned by varying the osmolyte concentration either in the microcapsule or the dispersed media, offering great flexibility in devising schemes for on-demand release in a precisely controlled manner. Also, we find that when the semi-permeable nature of the oil layer is combined with a hydrogel shell with varying thickness, the onset time of release can be controlled even under the same osmotic pressure. Furthermore, the hydrogel shell thickness can play a key role in controlling the release patterns to be either selective or simultaneous for multiple cargoes encapsulated in hydrogel microcapsules. We anticipate that further development in utilizing the two intermediate layers present in these hydrogel microcapsules will lead to a new pathway in designing functional hydrogel microcapsules with more complex and programmable release profiles.

4. Experimental Section

Materials: Polyethylene glycol diacrylate (PEGDA, M_n 700), poly(vinyl alcohol) (PVA, M_w 13 000-23 000, 87–89% hydrolyzed), 2,2-dimethoxy-2-phenylacetopheonon (photoinitiator), mineral oil, sucrose, erioglaucine disodium salt, fluorescein isothiocyanate-dextran

(M_w 20 000 000), doxorubicin hydrochloride (98%), hexadecane (99%), hexane (99%), ethanol (99%), FC-70, soybean oil, poly(ethylene glycol)-block-poly(propylene glycol)-block-poly(ethylene glycol) (Pluronic F-108, non-ionic surfactant, M_w 14 600) and trichloro(octadecyl) silane were purchased from Sigma–Aldrich. 2-[methoxy(polyethyleneoxy) propyl]trimethoxyl silane was purchased from Gelest. Krytox-PEG-Krytox (KPK) surfactant was purchased from Ran Biotechnology (Beverly, MA). Alexa Fluor 647 fibrinogen and Alexa Fluor 594 carboxylic acid tris(triethylammonium) salt and paclitaxel (Oregon Green 488 Conjugate) were purchased from Thermo Fisher Scientific. Deionized (DI) water (EXL 18.2 MΩ·cm at 28 °C) was used for all aqueous solutions. ABIL EM 90 was provided by Evonik Industry. Polyglycerol Polyricinoleate (PGPR) was provided from ILSHINWELLS CO. Square glass capillaries with an inner diameter of 1.05 mm were purchased from Atlantic International Technology (A.I.T.) and cylindrical glass capillaries with inner diameter of 0.58 mm and outer diameter of 1.00 mm were purchased from World Precision Instruments Inc. (W.P.I.). 5 min epoxy (Devcon) was used for assembling the glass capillary microfluidic devices. Microscope slide (3×1 inch, DURAN) and cover glass (Deckglaser) was used to fabricate custom-made chamber for micropipette aspiration.

Fabrication of Glass Capillary Microfluidic Device and Its Operation: An injection capillary was prepared by tapering a 580 µm inner diameter circular (cross-section) glass capillary to 100 µm inner diameter; to make the inner wall hydrophobic, the capillary was dipped in trichloro(octadecyl) silane for 10 min and subsequently washed with ethanol. The injection capillary was inserted into a square capillary whose inner width (1.05 mm) was slightly larger than that of the outer diameter of the injection capillary (1 mm). Next, a small tapered glass capillary (20 µm outer diameter) was prepared by pulling a cylindrical capillary; this capillary was inserted into the injection capillary for co-injection of two immiscible fluids (innermost and inner phases). Finally, a tapered collection capillary (Inner diameter of orifice: 350 µm) was inserted into the square capillary from the other end; this collection capillary was also treated with trichloro(octadecyl) silane to make the capillary wall hydrophobic. During drop generation, the volumetric flow rate was precisely controlled by syringe pumps (Legato100, KD Scientific) and the production of emulsion droplets was observed using an inverted fluorescence microscope (Eclipse Ti2, Nikon) equipped with a high-speed camera (MINI UX 50).

Characterization of Hydrogel Microcapsules: An inverted fluorescence microscope (Eclipse Ti2, Nikon) equipped with a CCD camera (sCMOS Zyla, Andor) was used to observe the resulting hydrogel microcapsules and image analysis of the particles was performed using the ImageJ (National Institute of Health) and NIS-Elements (Nikon) software programs. The time-dependent release patterns upon applying external stimulus were observed and characterized by confocal microscopy (SP-5, Leica). Osmolarity of all aqueous solutions was measured using a freeze point osmometer (Osmomet 3000, Gonotec) before use.

Quantitative Analysis of Doxorubicin Released from the Microcapsules: The doxorubicin concentration in each microcapsule suspension sample was measured using a UV–VIS spectrophotometer (UV-1800, Shimadzu) at room temperature. Five sets of microcapsule suspensions with varying number of microcapsules were prepared. The doxorubicin was released from the microcapsules and into the aqueous media upon destabilization of the oil layer in hypotonic condition. Theses aqueous solutions with varying concentration of doxorubicin were tranferred to quartz cuvette cells. UV–VIS spectra and calibration curve of doxorubicin were obtained at the maximum absorbance peak of doxorubicin ($\lambda_{max} \approx$ 485 nm) and paclitaxel ($\lambda_{max} \approx$ 227 nm). This procedure was repeated five times to obtain the error bars in the estimation of doxorubicin concentration.

Micropipette Aspiration Experiment: *Fabrication of the Micropipette*: Centimeter long tapered glass capillaries were obtained using a micropipette puller (P-97, Sutter Instrument). Then either ceramic tile or glass-to-glass technique was applied to obtain glass capillaries with inner diameters in the range of 60 to 80 µm.[42] These micropipettes were washed with deionized (DI) water and dried with house compressed

air using an air gun. After drying, silicone solution (Sigmacote, Sigma-Aldrich) was aspirated through the micropipette for silicone coating. Siliconized micropipettes were dried in an oven at 70 °C for 30 min and then rinsed with DI water several times.

Micropipette-Aspiration Setup: To measure the overall stiffness of the hydrogel microcapsules, a micropipette-aspiration setup was prepared by following the experimental setup described previously (Figure S4, Supporting Information).[43] The siliconized micropipette was fixed at one end of a custom-made chamber which comprised two square glass capillaries attached to a microscope slide and a cover glass placed on top.[44] These two square glass capillaries were spaced apart enough to fit a hydrogel microcapsule in between these capillaries. Then this custom-made chamber with the micropipette was placed on the stage of an inverted microscope (Eclipse Ti2, Nikon) equipped with a CMOS camera (Zyla 5.5, Andor). Prior to mounting on the inverted microscope, the micropipette was connected to a pressure pump through an intermediate liquid reservoir that could be moved perpendicularly. A syringe and a 3-way valve was located between the reservoir and the pipette to fill liquid into the tubing as well as the reservoir. A pressure pump (Fluigent, Flow-EZ) with 10 Pa resolution is used to apply negative suction pressure.

Experimental Methods: The tubing, reservoir, and the micropipette with 1 w/v% Pluronic F-108 aqueous solution were filled using a 3-way valve and syringe to prevent any change of osmotic pressure. Hydrogel microcapsules suspended in 1 w/v% Pluronic F-108 aqueous solution were then inserted in the custom-made chamber. After removing all the air bubbles in the system, the height of the intermediate reservoir and the pressure of microfluidic pump were carefully adjusted while monitoring the movement of debris floating in the chamber to determine the zero flux pressure inside the micropipette; the system was considered to be in zero flux condition when there was no movement of debris inside the micropipette. The pressure pump was then controlled to additionally introduce negative aspiration pressure with step increments of below 1 kPa. At each pressure step, the hydrogel microcapsule was allowed to equilibrate for about 60 s and aspirated length was acquired every few minutes by taking pictures of the microcapsule at designated aspiration pressure as shown in the series of optical micrographs of Figure S5, Supporting Information.

Data Processing and Image Analysis: ImageJ software was used to measure the aspirated length (L_p) and the radius of the micropipette opening (R_p) over each pressure step.[45] Two sets of hydrogel microcapsules were tested in which one set, denoted as thick shell, had shell thickness ranging from 15 to 19 μm while the other, thin shell had shell thickness of 5 to 7 μm. For each set of hydrogel microcapsules, at least five microcapsules were tested. The overall stiffness of microcapsule was determined from the slope of the deformation curve.[28] The typical deformation of the hydrogel microcapsule normalized to the inner pipette radius ($L_p–L_0)/R_p$ under negative aspiration pressure and their corresponding stiffness (slope) was shown in the plot of Figure S6, Supporting Information. The projection length of the capsule at zero pressure (L_0) was determined from the *y*-intercept of pressure versus total aspirated length (L_p).[28]

Supporting Information

Supporting Information is available from the Wiley Online Library or from the author.

Conflict of Interest

The authors declare no conflict of interest.

[1] a) C. S. Peyratout, L. Dahne, *Angew. Chem., Int. Ed.* **2004**, *43*, 3762; b) J. Wei, X.-J. Ju, X.-Y. Zou, R. Xie, W. Wang, Y.-M. Liu, L.-Y. Chu, *Adv. Funct. Mater.* **2014**, *24*, 3312.

[2] a) L. Kromidas, E. Perrier, J. Flanagan, R. Rivero, I. Bonnet, *Int. J. Cosmet. Sci.* **2006**, *28*, 103; b) J. Song, H. Chen, *Flavour Fragrance J.* **2018**, *33*, 160; c) W. Tangsongcharoen, P. Punyamoonwongsa, P. Chaiyasat, *Polym. Int.* **2019**, *68*, 714.

[3] M. V. Lomova, A. I. Brichkina, M. V. Kiryukhin, E. N. Vasina, A. M. Pavlov, D. A. Gorin, G. B. Sukhorukov, M. N. Antipina, *ACS Appl. Mater. Interfaces* **2015**, *7*, 11732.

[4] a) I. T. Carvalho, B. N. Estevinho, L. Santos, *Int. J. Cosmet. Sci.* **2016**, *38*, 109; b) J. Kozlowska, A. Kaczmarkiewicz, *Polym. Degrad. Stab.* **2019**, *161*, 108.

[5] a) Y. Wu, J. Shen, V. Larcinese-Hafner, P. Erni, L. Ouali, *RSC Adv.* **2016**, *6*, 102595; b) Y. Zhou, X. Han, X. Jing, Y. Chen, *Adv. Healthcare Mater.* **2017**, *6*, 1700646.

[6] a) F. Huang, W.-C. Liao, Y. S. Sohn, R. Nechushtai, C.-H. Lu, I. Willner, *J. Am. Chem. Soc.* **2016**, *138*, 8936; b) W.-C. Liao, M. Riutin, W. J. Parak, I. Willner, *ACS Nano* **2016**, *10*, 8683; c) C. H. Park, S. Lee, G. Pornnoppadol, Y. S. Nam, S.-H. Kim, B. J. Kim, *ACS Appl. Mater. Interfaces* **2018**, *10*, 9023.

[7] a) W. Meesorn, C. Calvino, J. C. Natterodt, J. O. Zoppe, C. Weder, *Adv. Mater.* **2019**, *31*, 1807212; b) T. Yim, M.-S. Park, S.-G. Woo, H.-K. Kwon, J.-K. Yoo, Y. S. Jung, K. J. Kim, J.-S. Yu, Y.-J. Kim, *Nano Lett.* **2015**, *15*, 5059.

[8] a) B. Mohanraj, G. Duan, A. Peredo, M. Kim, F. Tu, D. Lee, G. R. Dodge, R. L. Mauck, *Adv. Funct. Mater.* **2019**, *29*, 1807909; b) R. Rajamanickam, S. Baek, K. Gwon, Y. Hwang, K. Shin, G. Tae, *J. Mater. Chem. B* **2016**, *4*, 4278.

[9] C.-S. Hong, J. H. Park, S. Lee, K. Y. Rhoo, J. T. Lee, S. R. Paik, *ACS Appl. Mater. Interfaces* **2018**, *10*, 26628.

[10] a) E. Loiseau, A. Q. de Boiry, F. Niedermair, G. Albrecht, P. A. Rühs, A. R. Studart, *Adv. Funct. Mater.* **2016**, *26*, 4007; b) J. Yang, D. Katagiri, S. Mao, H. Zeng, H. Nakajima, S. Kato, K. Uchiyama, *J. Mater. Chem. B* **2016**, *4*, 4156.

[11] a) G. Duan, M. F. Haase, K. J. Stebe, D. Lee, *Langmuir* **2018**, *34*, 847; b) Q. Ma, Y. Song, J. W. Kim, H. S. Choi, H. C. Shum, *ACS Macro Lett.* **2016**, *5*, 666.

[12] A. C. Yu, L. M. Stapleton, J. L. Mann, E. A. Appel, in *Self-Assembling Biomaterials* (Eds: H. S. Azevedo, R. M. P. da Silva), Woodhead Publishing, Cambridge, UK **2018**, p. 205.

[13] T. D. Dao, H. M. Jeong, *Sol. Energy Mater. Sol. Cells* **2015**, *137*, 227.

[14] a) H. Li, S. Li, Z. Li, Y. Zhu, H. Wang, *Langmuir* **2017**, *33*, 14149; b) S. Tang, M. Yourdkhani, C. M. Possanza Casey, N. R. Sottos,

**ADVANCED
SCIENCE NEWS**

www.advancedsciencenews.com

**ADVANCED
FUNCTIONAL
MATERIALS**

www.afm-journal.de

S. R. White, J. S. Moore, *ACS Appl. Mater. Interfaces* **2017**, *9*, 20115; c) L. Zhao, X. Yang, Q. Li, L. Ma, *J. Appl. Polym. Sci.* **2019**, *136*, 47757.

[15] a) A. R. Abate, M. Kutsovsky, S. Seiffert, M. Windbergs, L. F. V. Pinto, A. Rotem, A. S. Utada, D. A. Weitz, *Adv. Mater.* **2011**, *23*, 1757; b) S.-H. Kim, D. A. Weitz, *Angew. Chem., Int. Ed.* **2011**, *50*, 8731; c) C. Nam, J. Yoon, S. A. Ryu, C.-H. Choi, H. Lee, *ACS Appl. Mater. Interfaces* **2018**, *10*, 40366; d) H. C. Shum, Y.-j. Zhao, S.-H. Kim, D. A. Weitz, *Angew. Chem., Int. Ed.* **2011**, *50*, 1648.

[16] a) A. Abbaspourrad, S. S. Datta, D. A. Weitz, *Langmuir* **2013**, *29*, 12697; b) A. M. DiLauro, A. Abbaspourrad, D. A. Weitz, S. T. Phillips, *Macromolecules* **2013**, *46*, 3309; c) Y. Zheng, Z. Yu, R. M. Parker, Y. Wu, C. Abell, O. A. Scherman, *Nat. Commun.* **2014**, *5*, 5772.

[17] a) Y. K. Jo, D. Lee, *Small* **2020**, *16*, 1903736; b) L. Liu, J.-P. Yang, X.-J. Ju, R. Xie, Y.-M. Liu, W. Wang, J.-J. Zhang, C. H. Niu, L.-Y. Chu, *Soft Matter* **2011**, *7*, 4821.

[18] a) W. J. Duncanson, T. Lin, A. R. Abate, S. Seiffert, R. K. Shah, D. A. Weitz, *Lab Chip* **2012**, *12*, 2135; b) T. Y. Lee, S. Lee, Y. H. Kim, D. J. Kim, E. Amstad, C.-S. Lee, S.-H. Kim, *Adv. Funct. Mater.* **2019**, *29*, 1902670; c) W. L. Lee, E. Widjaja, S. C. J. Loo, *Small* **2010**, *6*, 1003.

[19] C.-H. Choi, H. Lee, A. Abbaspourrad, J. H. Kim, J. Fan, M. Caggioni, C. Wesner, T. Zhu, D. A. Weitz, *Adv. Mater.* **2016**, *28*, 3340.

[20] H. Lee, C.-H. Choi, A. Abbaspourrad, C. Wesner, M. Caggioni, T. Zhu, S. Nawar, D. A. Weitz, *Adv. Mater.* **2016**, *28*, 8425.

[21] L. S. Roach, H. Song, R. F. Ismagilov, *Anal. Chem.* **2005**, *77*, 785.

[22] Z. Ye, F. Zhang, L. Han, P. Luo, J. Yang, H. Chen, *Colloids Surf.* **2008**, *322*, 138.

[23] A. Cavallo, M. Madaghiele, U. Masullo, M. G. Lionetto, A. Sannino, *J. Appl. Polym. Sci.* **2017**, *134*, 2.

[24] N. S. Heyman, J. M. Burt, *Biophys. J.* **2008**, *94*, 840.

[25] L. Wen, K. D. Papadopoulos, *J. Colloid Interface Sci.* **2001**, *235*, 398.

[26] S. N. Abd Jalil, D. K. Wang, C. Yacou, J. Motuzas, S. Smart, J. C. Diniz da Costa, *Materials* **2016**, *9*, 938.

[27] a) L. G. Alexopoulos, M. A. Haider, T. P. Vail, F. Guilak, *J. Biomech. Eng.* **2003**, *125*, 323; b) T. Aoki, T. Ohashi, T. Matsumoto, M. Sato, *Ann. Biomed. Eng.* **1997**, *25*, 581; c) T. Boudou, J. Ohayon, Y. Arntz, G. Finet, C. Picart, P. Tracqui, *J. Biomech.* **2006**, *39*, 1677.

[28] R. M. Kleinberger, N. A. D. Burke, K. Dalnoki-Veress, H. D. H. Stöver, *Mater. Sci. Eng. C* **2013**, *33*, 4295.

[29] L. Rolland, E. Santanach-Carreras, T. Delmas, J. Bibette, N. Bremond, *Soft Matter* **2014**, *10*, 9668.

[30] a) H. Lee, C.-H. Choi, A. Abbaspourrad, C. Wesner, M. Caggioni, T. Zhu, D. A. Weitz, *ACS Appl. Mater. Interfaces* **2016**, *8*, 4007; b) M. Wei, X. Pan, L. Rong, A. Dong, Y. He, X. Song, J. Li, *Mater. Res. Express* **2020**, *7*, 082001.

[31] a) D. Alonso, M. Gimeno, J. D. Sepúlveda-Sánchez, K. Shirai, *Carbohydr. Res.* **2010**, *345*, 854; b) P. S. Lee, S. G. Yim, Y. Choi, T. Van Anh Ha, S. Ko, *Food Chem.* **2012**, *134*, 992.

[32] a) S. An, M. W. Lee, A. L. Yarin, S. S. Yoon, *Chem. Eng. J.* **2018**, *344*, 206; b) M. M. Caruso, B. J. Blaiszik, H. Jin, S. R. Schelkopf, D. S. Stradley, N. R. Sottos, S. R. White, J. S. Moore, *ACS Appl. Mater. Interfaces* **2010**, *2*, 1195.

[33] S. Mohamaddoust Aliabadi, F. S. Mirzazadeh Tekie, O. Rajabi, M. R. Abbaspour, E. Khodaverdi, *Nanomed. J.* **2015**, *2*, 187.

[34] C. Li, J. Wang, Y. Wang, H. Gao, G. Wei, Y. Huang, H. Yu, Y. Gan, Y. Wang, L. Mei, H. Chen, H. Hu, Z. Zhang, Y. Jin, *Acta Pharm. Sin. B* **2019**, *9*, 1145.

[35] a) J. Li, D. J. Mooney, *Nat. Rev. Mater.* **2016**, *1*, 16071; b) M. Windbergs, Y. Zhao, J. Heyman, D. A. Weitz, *J. Am. Chem. Soc.* **2013**, *135*, 7933.

[36] T. Konno, J. Watanabe, K. Ishihara, *J. Biomed. Mater. Res.* **2003**, *65A*, 209.

[37] L. M. Diamante, T. Lan, *J. Food Process.* **2014**, *2014*, 1.

[38] T. Klein, S. Yan, J. Cui, J. W. Magee, K. Kroenlein, M. H. Rausch, T. M. Koller, A. P. Fröba, *J. Chem. Eng. Data* **2019**, *64*, 4116.

[39] L. Wen, K. D. Papadopoulos, *Colloids Surf., A* **2000**, *174*, 159.

[40] J. Bahtz, D. Z. Gunes, E. Hughes, L. Pokorny, F. Riesch, A. Syrbe, P. Fischer, E. J. Windhab, *Langmuir* **2015**, *31*, 5265.

[41] S.-H. Kim, J. W. Kim, J.-C. Cho, D. A. Weitz, *Lab Chip* **2011**, *11*, 3162.

[42] O. Adair, *Pipette Cookbook, Sutter Intrument*, Novato, CA **2018**.

[43] J.-L. Maître, R. Niwayama, H. Turlier, F. Nédélec, T. Hiiragi, *Nature Cell Biology* **2015**, *17*, 849.

[44] A. Mohammadalipour, M. M. Burdick, D. F. J. Tees, *FASEB J.* **2018**, *32*, 1806.

[45] J. Schindelin, I. Arganda-Carreras, E. Frise, V. Kaynig, M. Longair, T. Pietzsch, S. Preibisch, C. Rueden, S. Saalfeld, B. Schmid, J.-Y. Tinevez, D. J. White, V. Hartenstein, K. Eliceiri, P. Tomancak, A. Cardona, *Nat. Methods* **2012**, *9*, 676.